ARTICLE

Probenecid affects muscle Ca²⁺ homeostasis and contraction independently from pannexin channel block

Francisco Jaque-Fernandez[1], Bruno Allard[1], Laloé Monteiro[1], Aude Lafoux[2], Corinne Huchet[2,3], Enrique Jaimovich[4], Christine Berthier[1], and Vincent Jacquemond[1]

Tight control of skeletal muscle contractile activation is secured by the excitation–contraction (EC) coupling protein complex, a molecular machinery allowing the plasma membrane voltage to control the activity of the ryanodine receptor Ca²⁺ release channel in the sarcoplasmic reticulum (SR) membrane. This machinery has been shown to be intimately linked to the plasma membrane protein pannexin-1 (Panx1). We investigated whether the prescription drug probenecid, a widely used Panx1 blocker, affects Ca²⁺ signaling, EC coupling, and muscle force. The effect of probenecid was tested on membrane current, resting Ca²⁺, and SR Ca²⁺ release in isolated mouse muscle fibers, using a combination of whole-cell voltage-clamp and Ca²⁺ imaging, and on electrically triggered contraction of isolated muscles. Probenecid (1 mM) induces SR Ca²⁺ leak at rest and reduces peak voltage-activated SR Ca²⁺ release and contractile force by 40%. Carbenoxolone, another Panx1 blocker, also reduces Ca²⁺ release, but neither a Panx1 channel inhibitory peptide nor a purinergic antagonist affected Ca²⁺ release, suggesting that probenecid and carbenoxolone do not act through inhibition of Panx1-mediated ATP release and consequently altered purinergic signaling. Probenecid may act by altering Panx1 interaction with the EC coupling machinery, yet the implication of another molecular target cannot be excluded. Since probenecid has been used both in the clinic and as a masking agent for doping in sports, these results should encourage evaluation of possible effects on muscle function in treated individuals. In addition, they also raise the question of whether probenecid-induced altered Ca²⁺ homeostasis may be shared by other tissues.

Introduction

Skeletal muscle contraction and relaxation are determined by type 1 ryanodine receptor (RyR1)-mediated SR Ca²⁺ release and sarco-endoplasmic reticulum Ca²⁺-ATPase (SERCA)-mediated sarcoplasmic reticulum (SR) Ca²⁺ reuptake, respectively. RyR1 channel activity is under the control of the plasma membrane voltage through interactions with the $Ca_V1.1$ voltage-sensor; this molecular partnership constitutes the core of the excitation–contraction (EC) coupling machinery (Rebbeck et al., 2014; Hernandez-Ochoa et al., 2018; Rios, 2018). EC coupling is a very secure process, and there is actually a limited number of known pharmacological agents that can modify or disrupt its function so as to alter muscle force production in the intact organism (see Mackrill, 2010). Still, the possibility cannot be excluded that adverse effects of certain therapeutically approved molecules in the form of weakness and/or fatigue are related to the alteration of Ca²⁺ homeostasis and EC coupling.

Pannexins correspond to a family of three plasma membrane channel proteins (Panx1, 2, 3); Panx1 is so far the best characterized. It is ubiquitously expressed and exhibits a large, poorly selective pore allowing small molecules and is believed to mediate ATP release from the cytosol (see Dahl, 2015; Whyte-Fagundes and Zoidl, 2018). The recently solved cryo-EM structure of the Panx1 heptameric assembly has revealed the coexistence of a large conducting pathway together with seven additional chloride-conducting side tunnels, making the functional channel heptamer capable of passing ion current without necessary releasing ATP (Ruan et al., 2020). Panx1 is involved in a wide range of physiological and pathophysiological functions in different cell types (see Wang et al., 2013; Dahl, 2018). Accordingly, it is a therapeutic target of increasing interest for many pathological conditions, including infectious diseases, cancer, inflammation, and several diseases of the central

[1]Université Lyon, Université Claude Bernard Lyon 1, CNRS UMR-5261, INSERM U-1315, Institut NeuroMyoGène—Pathophysiology and Genetics of Neuron and Muscle, Lyon, France; [2]Therassay Platform, CAPACITES, Université de Nantes, Nantes, France; [3]Nantes Gene Therapy Laboratory, Université de Nantes, INSERM UMR 1089, Nantes, France; [4]Centro de Estudios Moleculares de la Célula, Instituto de Ciencias Biomédicas, Facultad de Medicina, Universidad de Chile, Santiago, Chile.

Correspondence to Vincent Jacquemond: vincent.jacquemond@univ-lyon1.fr.

nervous system (e.g., Dahl and Keane, 2012; Eugenin, 2014; Navis et al., 2020; Vultaggio-Poma et al., 2020; Giaume et al., 2021).

Skeletal muscle activity is associated with ATP release into the interstitial space (Li et al., 2008), with potential downstream autocrine and paracrine functions through purinergic receptors (e.g., Nyberg et al., 2013; Ito et al., 2018). Several lines of evidence have promoted a function for Panx1-mediated ATP release and consequent autocrine activation of purinergic signaling in the control of muscle plasticity (Buvinic et al., 2009; Jorquera et al., 2013; Bustamante et al., 2014). This process operates in an action potential frequency-dependent manner, sensed and transduced by $Ca_V1.1$ to Panx1 (Casas et al., 2010; Jorquera et al., 2013). Consistently, a multiprotein complex including $Ca_V1.1$, Panx1, and P2Y2 has been described (Arias-Calderón et al., 2016).

The close molecular and functional interactions between the EC coupling machinery and Panx1 led us to postulate that altering Panx1 function may affect intracellular Ca^{2+} handling and EC coupling. To address this issue, we focused on a molecule classically used to block Panx1, probenecid, which has also been used for clinical purposes. We show that probenecid affects resting Ca^{2+} homeostasis, voltage-activated Ca^{2+} release, and whole muscle force production. Preliminary aspects of this work have been presented in an abstract form (Jaque-Fernandez et al., 2022).

Materials and methods

Experiments were performed following the ethics principles of the French Department of Veterinary Services and the French Ministry for Higher Education, Research and Innovation; in accordance with the guidelines of the local committees in charge of animal well-being (SBEA) at University Claude Bernard Lyon 1 and at University of Nantes, the French Ministry of Agriculture (decree 87/848), and the revised European Directive 2010/63/EU. Animals were housed at the accredited Therassay (University of Nantes) and Aniphy (University Lyon 1) animal facilities. Experimental design and analysis and their reporting followed ARRIVE 2.0 (Percie du Sert et al., 2020) and BJP guidelines (Curtis, 2018). Experiments were performed on muscles and muscle fibers isolated from mice as basic aspects of the physiology of EC coupling in human muscles (Garcia et al., 1992; Struk et al., 1998) are similar to those in mouse muscles (Collet et al., 2004; Hernandez-Ochoa and Schneider, 2012).

Isolation and preparation of muscle fibers for voltage-clamp
Single fibers were isolated from the flexor digitorum brevis muscles of 8–12-wk-old OF1 male mice (Charles River). OF1 mice were used because dense sets of healthy, robust muscle fibers can be isolated in a very reproducible manner from this strain which, over the years, has become a standard model in our laboratory. Procedures were as described previously (Jacquemond, 1997; Lefebvre et al., 2011). In brief, mice were anesthetized by isoflurane inhalation and killed by cervical dislocation. Muscles were removed and incubated for 60 min at 37°C in the presence of Tyrode solution containing 2 mg/ml of

collagenase (Sigma-Alrich, type 1). Single intact muscle fibers were then released by gentle mechanical trituration of the enzyme-treated muscles. Trituration was achieved within the experimental chamber: a 50-mm wide culture μ-dish (Ibidi), in the presence of culture medium containing 10% bovine fetal serum (MI199; Eurobio). Prior to trituration, the bottom of the chamber had been covered with a thin layer of silicone grease. This enabled single fibers to be covered with additional silicone so that a 50–100-μm-long portion of the fiber extremity was left out, as previously described (Jacquemond, 1997). The culture medium solution was replaced by our standard extracellular solutions (see Solutions). The tip of a glass micropipette filled with an intracellular-like solution containing a Ca^{2+}-sensitive dye (see Solutions) was inserted into the silicone-embedded fiber portion. The silver–silver chloride wire inside the micropipette was connected to an RK-400 patch-clamp amplifier (Bio-Logic) used in whole-cell voltage-clamp configuration. Command voltage pulse generation was achieved with an analog-digital converter (Digidata 1440A, Axon Instruments) controlled by pClamp 9 software (Axon Instruments). The tip of the micropipette was gently crushed against the bottom of the chamber to reduce the series resistance. Analog compensation was adjusted to further decrease it. Unless otherwise specified, voltage-clamp steps were applied from a holding command potential of –80 mV. In the experiments designed to test the effect of probenecid and carbenoxolone using the preincubation protocol (see Solutions), an estimate of the amount of $Ca_V1.1$ intramembrane charge movement was made by analyzing the depolarization-induced changes in membrane current according to previously described procedures (e.g., Jaque-Fernández et al., 2021). For this, changes in current elicited by –20 mV pulses delivered before each test depolarizing pulse were averaged and used as a control for subtracting the linear components. As the experiments were performed in a calcium-containing extracellular solution, contamination by the $Ca_V1.1$ Ca^{2+} current was limiting. Thus, only the "ON" portion of the current transients was used and the amount of charge measured from the corrected current records was made with integration limited to 5 ms after the onset of the depolarizing pulses. The corresponding calculated charge was normalized to the capacitance of the fiber. All experiments were performed at room temperature (20–22°C).

Ca^{2+} imaging
Detection of fluorescence from the Ca^{2+}-sensitive dye dialyzed into the fiber's cytosol was achieved with a Zeiss LSM 800 microscope equipped with a 63× oil immersion objective (numerical aperture 1.4). Standard green and red configurations were used for detection of the fluorescence of fluo-4 and rhod-2, respectively. Voltage-activated fluorescence changes were imaged using the line-scan mode (x,t) of the system. They were expressed as F/F_0 with F_0 as the baseline fluorescence. In experiments designed to follow the effect of probenecid after acute application of the drug, the changes in resting fluorescence F_0 were normalized to F_0 in the control condition at the beginning of the experiment; this value is referred to as $_{intial}F_0$. In graphs presenting fluorescence transients, the y-scale bar corresponds to the indicated multiple of F_0. Quantification of the Ca^{2+} release

flux (dCa_{Tot}/dt) underlying the rhod-2 Ca^{2+} transients was performed as previously described (Lefebvre et al., 2011; Kutchukian et al., 2016). The resting Ca^{2+} concentration was assumed to be 100 nM in all conditions, except for results shown in Figs. 8 and 9, for which the change in resting Ca^{2+} concentration induced by probenecid was implemented in the Ca^{2+} release flux calculation. For this, the resting Ca^{2+} level in the presence of probenecid was calculated from the increase in resting fluorescence, assuming an initial resting $[Ca^{2+}]$ level of 0.1 µM, and F_{max}/F_{min} and K_D values for rhod-2 of 30 and 1.63 µM, respectively (Sanchez et al., 2021). The voltage-dependence of the peak Ca^{2+} release flux from each muscle fiber was fitted with a Boltzmann function:

$$\frac{dCa_{Tot}}{dt} = \frac{Max\frac{dCa_{Tot}}{dt}}{\{1 + \exp[(V_{0.5} - V)/k]\}},$$

with $Max\ dCa_{Tot}/dt$ the maximum Ca^{2+} release flux, $V_{0.5}$ the mid-activation voltage, and k the steepness factor.

Muscle force measurements

Electrically stimulated isolated extensor digitorum longus (EDL) muscles were used to assess the effect of probenecid on force development. For this, 8-wk-old OF1 male mice were anesthetized by isoflurane inhalation and killed by cervical dislocation, and EDL muscles were removed. Force measurements were performed using the 1205A Isolated Muscle System from Aurora Scientific. The EDL muscle was mounted in the experimental chamber in the presence of air-bubbled Ringer solution (see Solutions) maintained at 25°C. The muscle was stretched to the optimum length for the production of maximum isometric twitch force triggered by a supra-maximum 0.2-ms-long electrical stimulation. From this time point, the muscle was repeatedly stimulated by a series of five such electrical stimulations applied at 0.1 Hz, every 5 min, throughout the experiment. Force measurements were performed in response to 60 Hz supramaximum tetanic trains of stimulations of 0.5 s total duration, applied every 15 min. Following the first tetanic response, the Ringer solution was exchanged for the DMSO-containing Ringer with or without probenecid. Force values were normalized by the weight of the muscle.

Solutions

Tyrode solution contained (in mM) 140 NaCl, 5 KCl, 2.5 CaCl$_2$, 2 MgCl$_2$, and 10 HEPES. The standard extracellular solution for voltage-clamp experiments contained (in mM) 140 TEA-methane-sulfonate, 2.5 CaCl$_2$, 2 MgCl$_2$, 1 4-aminopyridine, 10 HEPES, and 0.002 tetrodotoxin. For the experiments described in Figs. 1 and 2, the extracellular solution also contained 0.33% DMSO. The standard pipette solution contained (in mM) 120 K-glutamate, 5 Na$_2$-ATP, 5 Na$_2$-phosphocreatine, 5.5 MgCl$_2$, 5 glucose, and 5 HEPES. For measurements of rhod-2 Ca^{2+} transients, it also contained 15 EGTA, 6 CaCl$_2$, and 0.1 rhod-2. For measurements with fluo-4, isolated muscle fibers were incubated for 30 min in the presence of Tyrode solution containing 10 µM fluo-4 AM. All solutions were adjusted to pH 7.20. The Ringer solution used for muscle force measurements contained

(in mM) 140 NaCl, 6 KCl, 3 CaCl$_2$, 2 MgCl$_2$, and 10 HEPES, adjusted to pH 7.40.

Probenecid was prepared as a 0.3 M aliquoted stock solution in DMSO and used in the extracellular solution at 0.5, 1, or 2 mM. Carbenoxolone was prepared as a 10 mM stock solution in the extracellular solution and used at 0.1 mM. These concentrations were chosen on the basis of their effectiveness and wide use to block Panx1 channels throughout the literature (e.g., Dahl et al., 2013). When testing the effect of either probenecid or carbenoxolone using the preincubation protocol (Figs. 1 and 2), fibers were bathed in the drug-containing extracellular solution from the beginning of the intracellular dialysis with the rhod-2-containing solution (i.e., 30 min before taking measurements). The [10]panx1 peptide and the scrambled control peptide ([10]panx1SCr) were tested under the same conditions at 200 µM while the P2Y2 antagonist AR-C 118925XX was tested at 10 µM. All chemicals and drugs were purchased from Sigma-Aldrich, except for tetrodotoxin (Alomone Labs), rhod-2 and fluo-4 (Thermo Fisher Scientific), and AR-C 118925XX (TOCRIS—Bio-Techne).

In vitro fluorescence measurements using droplets of a solution containing (in mM) 120 K-glutamate, 10 HEPES, 15 EGTA, 6 CaCl$_2$, and 0.1 rhod-2, with or without probenecid, showed that fluorescence intensity in the presence of 1 mM probenecid corresponded to 1.09 ± 0.12% ($n = 6$) the intensity in the absence of probenecid, excluding an interaction of the drug with the dye to explain the effect on resting fluorescence in muscle fibers.

Data and statistical analysis

During the experiments, muscle fibers and muscles were randomly assigned to the control and test (probenecid, carbenoxolone, or other treatment) groups. When comparing results between control muscle fibers and muscle fibers treated under a given pharmacological condition, groups of fibers from the same animal were considered as technical replicates and statistical comparison was achieved using a nested analysis, as described by Eisner (2021). When determining the extent of change in a given parameter produced by the acute application of a pharmacological compound (with the initial measurement from the same muscle or muscle fiber being the control value), each experiment was considered independent, and statistics were based on the number of fibers.

The number of necessary experiments was estimated on the basis of our previous experience with each protocol. A sample size estimation (with $\alpha = 0.05$ and $\beta = 0.80$) was made from our pilot data showing a 55% reduction of maximum SR Ca^{2+} release in the presence of 1 mM probenecid, giving a total of six per group.

Experiments on single muscle fibers and isolated muscles require a great extent of specific expertise, preparation, dexterity, and watchfulness, with the operator on duty being in charge from beginning to end. Under these conditions, further complexification by blinding was not implemented to prevent any related risk of misidentification error. Blinding would also have required two dedicated persons on duty on each experimental day, which was not routinely possible.

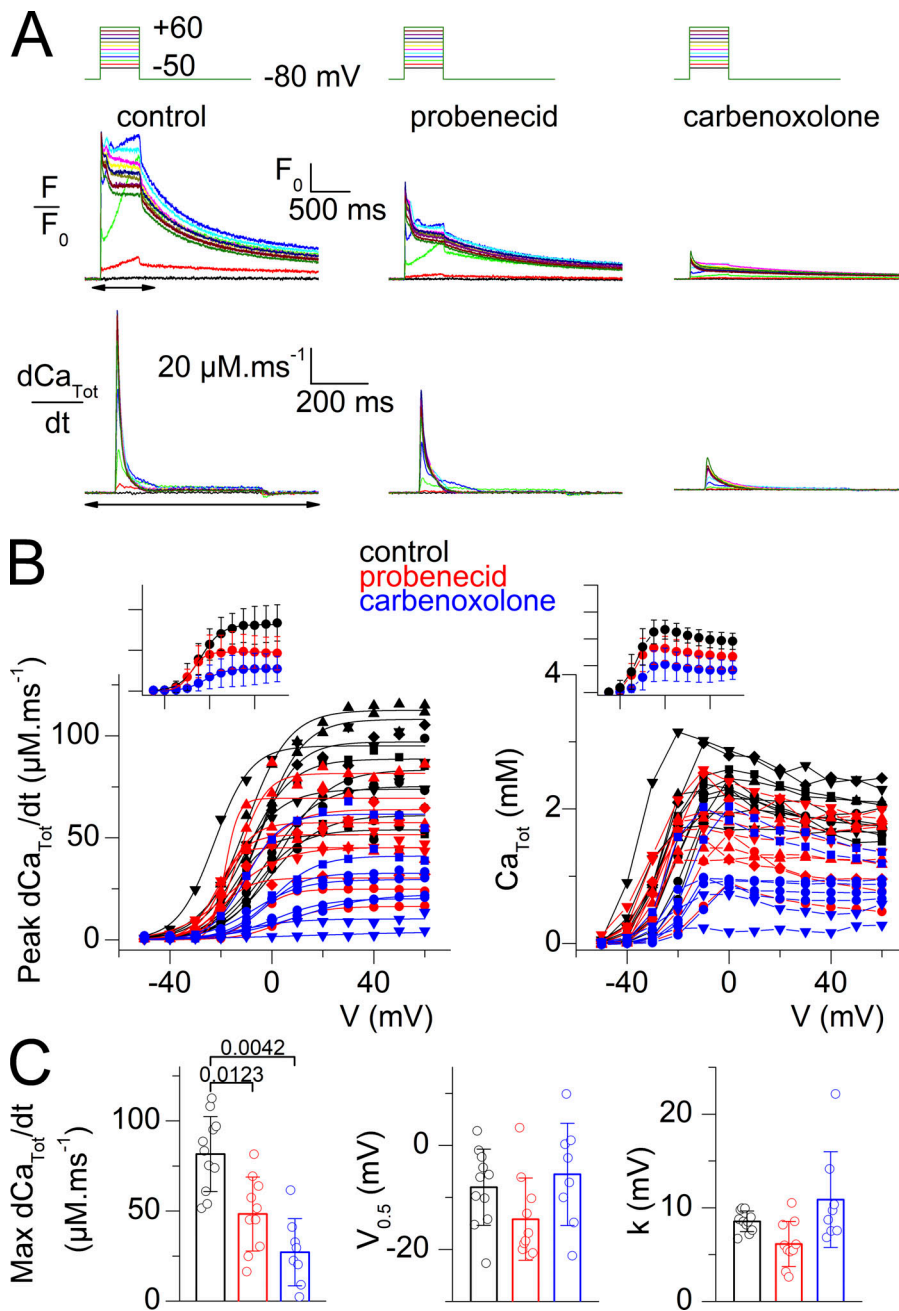Data and statistical analysis complied with the recommendations on experimental design and analysis in

Figure 1. **Probenecid and carbenoxolone depress voltage-activated SR Ca²⁺ release.** (A) Representative examples of rhod-2 fluorescence transients (F/F$_0$ traces) and corresponding calculated SR Ca²⁺ release flux (dCa$_{Tot}$/dt) elicited by the voltage-clamp pulse protocol shown on top, in a control fiber, in a fiber equilibrated in the presence of probenecid, and in a fiber equilibrated in the presence of carbenoxolone. (B) Voltage-dependence of the peak amplitude of SR Ca²⁺ release (left) and of the corresponding total amount of released Ca²⁺ (right) in the control group of fibers (black) and in the groups of fibers treated with probenecid (red) and carbenoxolone (blue), all tested as shown in A. Individual datapoints from each muscle fiber are shown, with the corresponding Boltzmann fit superimposed (continuous line). An identical symbol is used for fibers from the same mouse. The control, probenecid, and carbenoxolone datasets are from 11 fibers from six mice, 10 fibers from four mice, and 8 fibers from three mice, respectively. Data from muscle fibers issued from the same mouse are shown with the same symbol. The inset in each panel shows the corresponding mean (±SD) values in each group with the x and y scale covering the same ranges as in the main panel. (C) Individual and mean (±SD) values for the Boltzmann parameters in the three groups of muscle fibers. Statistical difference between the parameters in the control and either the probenecid or the carbenoxolone groups was assessed using the nested analysis described by Eisner (2021).

pharmacology (Curtis et al., 2018). Electrophysiological and fluorescence data were processed with Clampfit 10.0 (Molecular Devices) and ImageJ software (National Institutes of Health), respectively, and Origin 7.0 (OriginLab Corporation). Statistical analysis was performed with GraphPad Prism 9.1 (GraphPad Software). Data values are presented as means ± SD for either n muscle fibers or n muscles. Individual datapoints for the parameters measured from each and every muscle/fiber tested are also presented in the figures. Statistical comparison was made only on measurements conducted under a given experimental condition on a minimum group of either five distinct muscles or five distinct muscle fibers. No search was made for outliers within datasets. The level of probability (p) deemed to constitute the threshold for statistical significance

was defined as P < 0.05. Exact P values are indicated on the graphs in the figures.

For single muscle fiber experiments designed to test the effect of chronic exposure to a pharmacological compound (Figs. 1, 2, and 4), the normality of the distribution of each Boltzmann fit parameter was assessed using Shapiro-Wilk test, and the statistical difference between the control group and either the probenecid group or the carbenoxolone group was determined using the hierarchical (nested) analysis or linear mixed modeling described by Eisner (2021), taking into account the number of fibers from each mouse.

For single muscle fiber experiments designed to test the effect of acute exposure to probenecid, statistical differences between the control group and the probenecid group in terms of
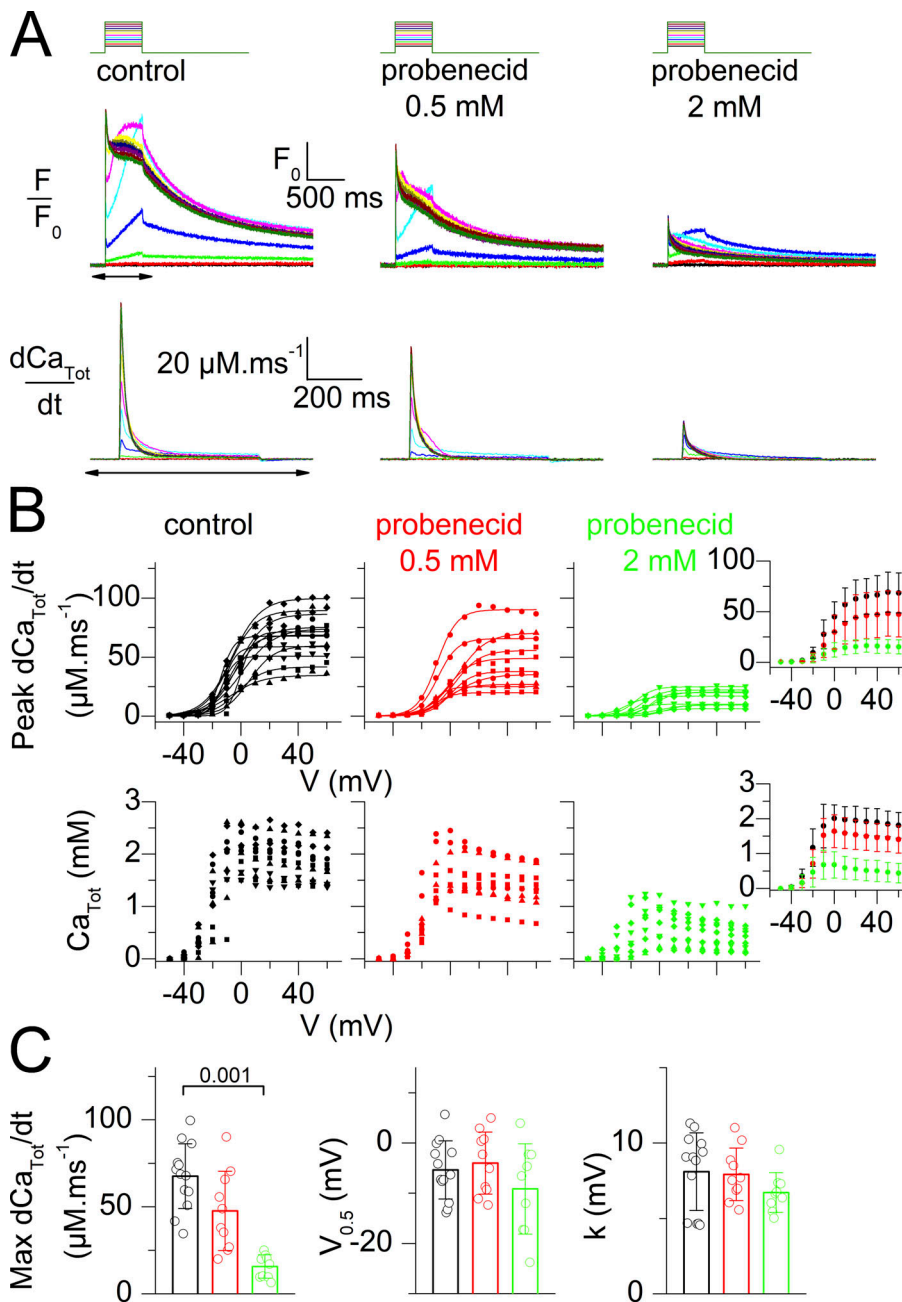
Figure 2. Effect of probenecid at 0.5 and at 2 mM on voltage-activated SR Ca²⁺ release. (A) Representative examples of rhod-2 fluorescence transients (F/F_0 traces) and corresponding calculated SR Ca²⁺ release flux (dCa_{Tot}/dt) elicited by the voltage-clamp pulse protocol shown on top, in a control fiber, in a fiber equilibrated in the presence of 0.5 mM probenecid, and a fiber equilibrated in the presence of 2 mM probenecid. **(B)** Voltage-dependence of the peak amplitude of SR Ca²⁺ release (dCa_{Tot}/dt, top panels) and of the corresponding total amount of released Ca²⁺ (Ca_{Tot}, bottom panels) in the control group of fibers (black) and the groups of fibers treated with probenecid (red and green), all tested as shown in A. Individual datapoints from each muscle fiber are shown, with the corresponding Boltzmann fit superimposed (continuous line). The control, probenecid 0.5 mM, and probenecid 2 mM datasets are from 13 fibers from five mice, 10 fibers from three mice, and 9 fibers from three mice, respectively. Data from muscle fibers issued from the same mouse are shown with the same symbol. The inset on the right in each panel shows corresponding mean (±SD) values in each group with the *x* and *y* scale covering the same ranges as in the main panel. **(C)** Individual and mean (± SD) values for the Boltzmann parameters in the three groups of muscle fibers. Statistical difference between the parameters in the control and either the probenecid or the carbenoxolone groups was assessed using a nested analysis (Eisner, 2021).

the extent of change in (1) baseline rhod-2 fluorescence, (2) resting membrane conductance, and (3) peak SR Ca²⁺ release flux during the test period and after wash-out, was assessed using unpaired Mann–Whitney Wilcoxon test (Figs. 6 and 9).

For muscle force measurements in control conditions and in the presence of probenecid, a Mann–Whitney Wilcoxon test was used to compare the amplitude of tetanic force at a given time point of the experiment. Friedman's nonparametric test for repeated measurements followed by Dunn's post-hoc test was used to compare the time-dependent changes in the tetanic force amplitude in the two groups.

Results

Depressed SR Ca²⁺ release in muscle fibers incubated in the presence of either probenecid or carbenoxolone

The effect of probenecid (1 mM) and carbenoxolone (0.1 mM) on EC coupling was first tested in steady-state conditions using a preincubation protocol. For this, voltage-activated Ca²⁺ transients were measured from fibers bathed either in the absence or in the presence of one of the two drugs and challenged by 0.5-s long depolarizing pulses of increasing amplitude. Representative rhod-2 F/F_0 traces from one fiber of each group, all from the same mouse, are shown in Fig. 1 A, with traces underneath
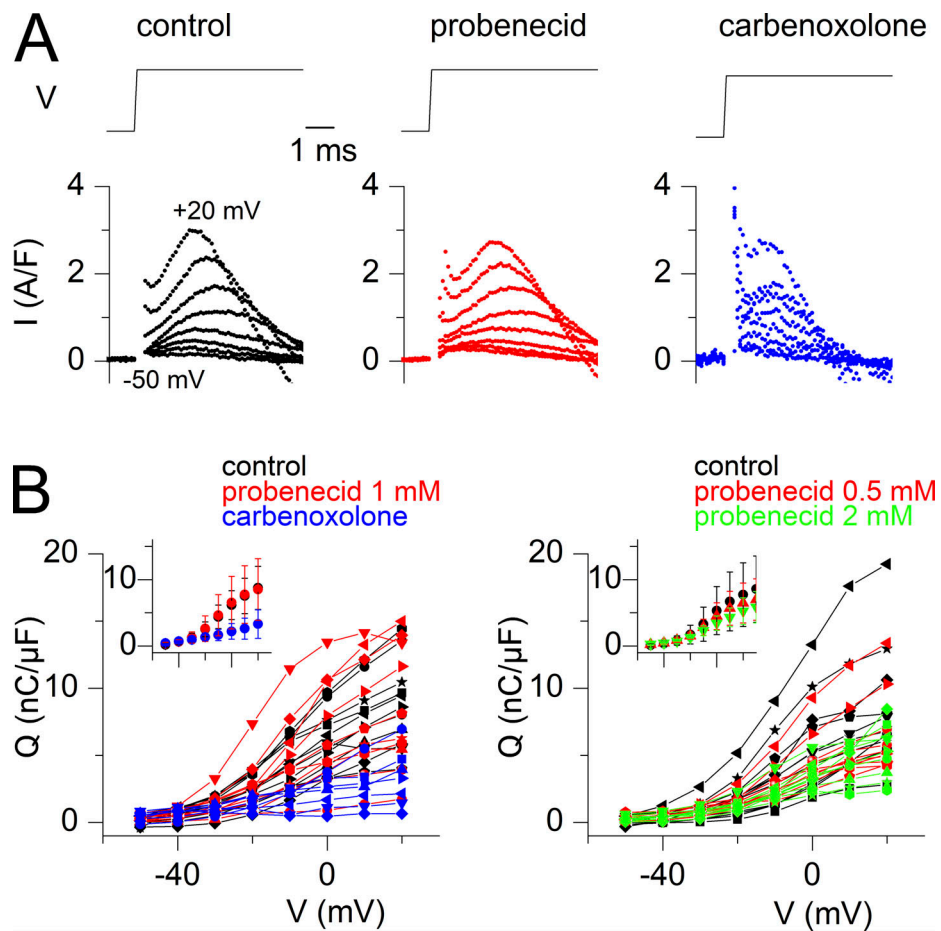
Figure 3. **Estimation of charge movement in probenecid- and carbenoxolone-treated fibers. (A)** Examples of charge movement current traces elicited at the onset of depolarizing pulses to values ranging between −50 and +20 mV in a control fiber, in a fiber treated with 1 mM probenecid and in a fiber treated with 100 μM carbenoxolone. **(B)** Voltage dependence of the charge density in all fibers tested under the indicated conditions. Insets show corresponding mean (±SD) values. Data are from the same fibers as in Fig. 1 (left) and Fig. 2 (right).

corresponding to the SR Ca^{2+} release flux (dCa_{Tot}/dt) with an expanded time scale (time period corresponding to that indicated by a double-arrow below the control F/F_O traces). The probenecid- and carbenoxolone-treated fibers generated Ca^{2+} transients of smaller amplitude than the control fiber due to a reduced peak SR Ca^{2+} release flux at all voltages. Values for peak dCa_{Tot}/dt, versus voltage in all tested fibers are shown in the left panel of Fig. 1 B. The inset shows mean values in each group. Despite fiber-to-fiber variability, results indicate that probenecid and carbenoxolone depress voltage-induced RyR1-mediated SR Ca^{2+} release, with carbenoxolone yielding the most severe effect. Fig. 1 C shows corresponding mean values for the Boltzmann fit parameters, with values from each fiber superimposed. Statistical analysis (see Materials and methods) showed that the maximum SR Ca^{2+} release flux was reduced by ∼40% in the probenecid group and ∼70% in the carbenoxolone group, as compared with the control group. Values for the $V_{0.5}$ and for k did not statistically differ. Thus, probenecid and carbenoxolone depress SR Ca^{2+} release without affecting the sensitivity to the membrane voltage of the process.

In a separate series of experiments under the same conditions, probenecid was found to have no significant effect on maximum SR Ca^{2+} release at 0.5 mM, while reducing it by >70% at 2 mM (Fig. 2).

The right panel in Fig. 1 B shows corresponding values, in each fiber, for the total amount of Ca^{2+} released (Ca_{Tot}), with the inset showing the mean values from all fibers. This parameter, calculated from the running integral of the release flux, was also depressed in the presence of either of the two drugs, as compared with the control condition (see also Fig. 2 B, bottom graphs).

To estimate whether depression of SR Ca^{2+} release by probenecid and carbenoxolone may result from a defect of $Ca_V1.1$ charge movement, we analyzed the changes in membrane current following the onset of the depolarizing pulses from fibers used in Figs. 1 and 2 (see Material and methods). Examples of charge movement currents in a control fiber, in a fiber treated with 1 mM probenecid, and in a fiber treated with carbenoxolone are shown in Fig. 3 A, whereas Fig. 3 B shows the voltage-dependence of the so-estimated charge density for each fiber in Fig. 1 (left graph) and Fig. 2 (right graph). There was no indication that probenecid, at the three tested concentrations, affected charge movement. Conversely, the amount of charge was reduced in the carbenoxolone-treated fibers. For instance, with
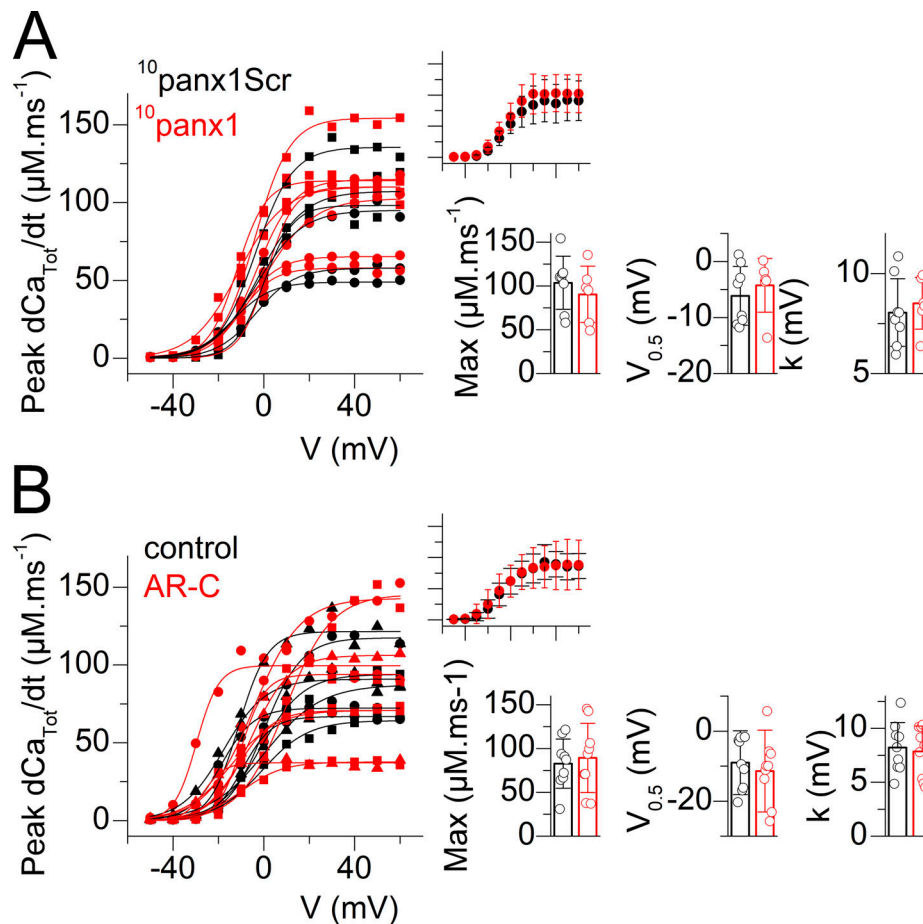
Figure 4. **The Panx1 inhibitory peptide [10]panx1 and the P2Y2 antagonist AR-C118925 do not affect voltage-activated SR Ca^{2+} release. (A)** Voltage dependence of the peak amplitude of SR Ca^{2+} release in fibers treated with 200 µM of either the [10]panx1 peptide (red) or with the scrambled control peptide ([10]panx1SCr, black). Individual datapoints from each muscle fiber are shown, with the corresponding Boltzmann fit superimposed (continuous line). The [10]panx1SCr and [10]panx1 datasets are from six fibers and four fibers from two mice, respectively. Data from muscle fibers issued from the same mouse are shown with the same symbol. The inset on the right shows the corresponding mean (±SD) values in each group with the x and y scale covering the same ranges as in the main panel. Individual and mean (±SD) values for the Boltzmann parameters in the two groups of muscle fibers are shown in the bar graphs. The absence of statistical difference between the parameters in the two groups was assessed using a nested analysis (Eisner, 2021). **(B)** Voltage dependence of the peak amplitude of SR Ca^{2+} release in control fibers (black) and in fibers treated with 10 µM of AR-C118925 (red). Individual datapoints from each muscle fiber are shown, with the corresponding Boltzmann fit superimposed (continuous line). The control and AR-C118925 datasets are from nine fibers and nine fibers from three mice. Data presentation and analysis are as described in A.

respect to the dataset in Fig.1, mean (±SD) values for charge density in response to a pulse to +20 mV were 7.5 ± 2.7, 7.8 ± 4.3, and 2.6 ± 1.6 nC/µF in control fibers (n = 11), in fibers treated with 1 mM probenecid (n = 10), and in fibers treated with carbenoxolone (n = 7), respectively. Statistical analysis showed that values did not differ between the control and the probenecid group, whereas the carbenoxolone group exhibited significantly lower values than the control group. Although we need to remain careful with these conclusions because experimental conditions were limiting for such analysis (see Materials and methods), it at least provides no indication that probenecid affected $Ca_V1.1$ charge movement, whereas in contrast, carbenoxolone may do so.

In order to determine whether depression of SR Ca^{2+} release is an obligatory consequence of Panx1 channel block, we used the specific inhibitory peptide [10]panx1 (Pelegrin and Surprenant, 2006). Exposure of muscle fibers to [10]panx1 (200 µM) under the same conditions as probenecid or carbenoxolone (Fig. 1) did not affect SR Ca^{2+} release (Fig. 4 A). Thus, probenecid and carbenoxolone are likely affecting Ca^{2+} release independently from their capacity to block ATP exit through Panx1.

We also tested whether probenecid-induced blockade of purinergic signaling is involved by treating fibers with a P2Y receptor antagonist. Since evidence was provided that the P2Y2 receptor is part of a multiprotein complex including $Ca_V1.1$ and Panx1 (Buvinic et al., 2009; Arias-Calderon et al., 2016), we focused our efforts on testing the P2Y2 specific antagonist AR-C118925. Results shown in Fig. 4 B show that the antagonist had no effect on SR Ca^{2+} release.

Acute application of probenecid releases stored Ca^{2+}

Results from Figs. 1 and 2 prompted us to determine whether depression of Ca^{2+} release was associated with other chronic or transient changes that may be hard to reveal from comparison of
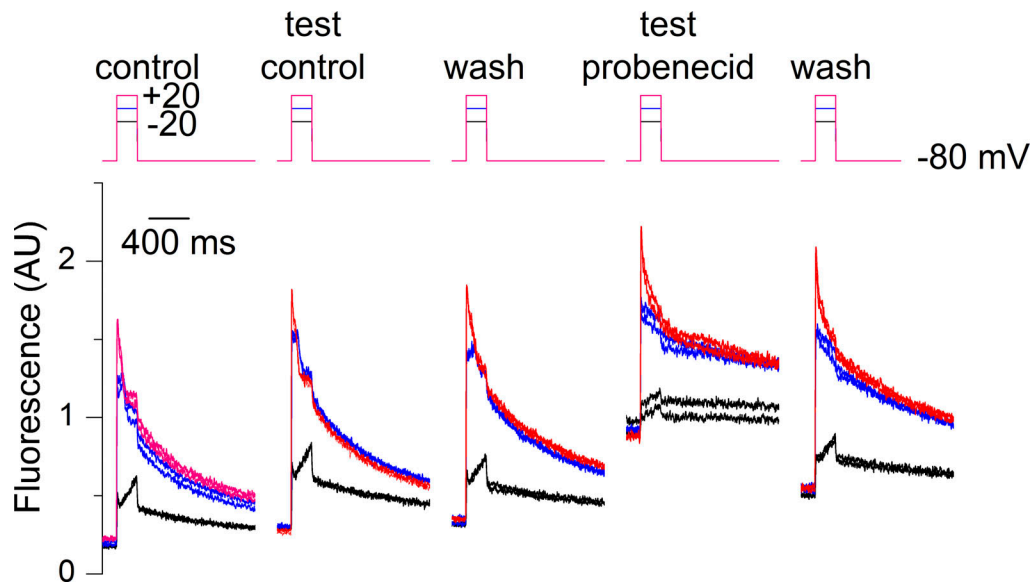
Figure 5. **Effect of a transient application of probenecid on voltage-activated Ca²⁺ transients in a muscle fiber.** Rhod-2 Ca²⁺ transients elicited by the pulse protocol shown on top upon successive changes in the extracellular solution. Each depolarizing pulse was repeated twice to check for the stability of the response. From left to right, rhod-2 transients elicited by 200 ms-long pulses to –20, 0, and +20 mV (1) in the initial control condition, (2) during the test-control condition, (3) after wash out (wash), (4) after application of the probenecid-containing solution, and finally after probenecid wash-out. Throughout the control measurements, the resting rhod-2 fluorescence level tended to slightly increase with time because of the not-entirely-complete (1) equilibration of the pipette solution with the cell interior and (2) recovery of the resting fluorescence following a voltage-activated transient.

data between a control group and a treated group of fibers at steady state. In the following sections, we specifically focused on probenecid because of the potential clinical relevance of the effects. A protocol of transient probenecid application was used, which also allowed testing the reversibility of the effects; voltage-activated rhod-2 Ca²⁺ signals were measured in the same fiber, in control conditions, after applying probenecid and then after probenecid wash-out.

Since measuring SR Ca²⁺ release in response to repeated depolarizing pulses, together with extracellular solution changes, is a challenging experimental situation, we performed an identical series of control experiments through which the DMSO-only containing extracellular solution was applied to the fibers (referred to as test-control protocol).

Fig. 5 shows an example of data collected from one fiber challenged first with a test-control protocol and then with probenecid. Probenecid triggered a steep increase in baseline fluorescence accompanied by a reduction in the amplitude of the rhod-2 transients. Both effects tended to be reversed upon probenecid wash-out. This provides a compelling indication that probenecid affects resting intracellular Ca²⁺ homeostasis. Because completing an entire set of measurements, on a same fiber, as in Fig. 5, was hard to achieve, we relied instead on the comparison of data between a group of fibers experiencing the test-control protocol and a group of fibers challenged with probenecid.

Under these conditions, we first focus here on the resting rhod-2 fluorescence. The evolution of this parameter over the course of each experiment is shown in Fig. 6 A. Black and red correspond to data from fibers challenged with the control protocol and with the probenecid protocol, respectively. For

each fiber, all prepulse baseline fluorescence levels were normalized to the baseline value measured before the first pulse was applied (referred to as $_{initial}F_0$). The inset in Fig. 6 A shows the raw data while the main panel shows the same data after normalizing each dataset by a linear function fitted to the data points before the application of probenecid and extrapolated to the entire set. This normalization was intended to correct for the slow rise in fluorescence over time (see Fig. 5). It was not entirely satisfactory over the full experiment's duration as most $F_0/_{initial}F_0$ values tended to decline with time. Nevertheless, results clearly show that probenecid reproducibly and reversibly enhanced resting rhod-2 fluorescence. The bar graphs at the bottom of Fig. 6 A show the mean values for $F_0/_{initial}F_0$ during the application of probenecid (or during the corresponding period for the control fibers) and after wash-out. Statistical analysis established a significant rise in resting fluorescence in the probenecid-treated group of fibers, as compared with the control group, whereas there was no difference after wash. Using calibration values given in Materials and methods, probenecid was estimated to elevate the resting Ca²⁺ from an assumed initial level of 0.1 µM to a mean level of 0.23 ± 0.09 µM ($n = 9$).

The above results suggest that a rise in resting Ca²⁺ is accompanying the depressing effect of probenecid on voltage-activated SR Ca²⁺ release. We excluded that the fluorescence rise would result from an increased rhod-2 concentration due to probenecid-induced inhibition of rhod-2 leakage out of the fiber. This possibility could be raised because probenecid was shown to block extracellular leakage of calcium-sensitive dyes (e.g., Di Virgilio et al., 1988). In our conditions, baseline rhod-2 fluorescence increased on average by a factor of 1.7 within
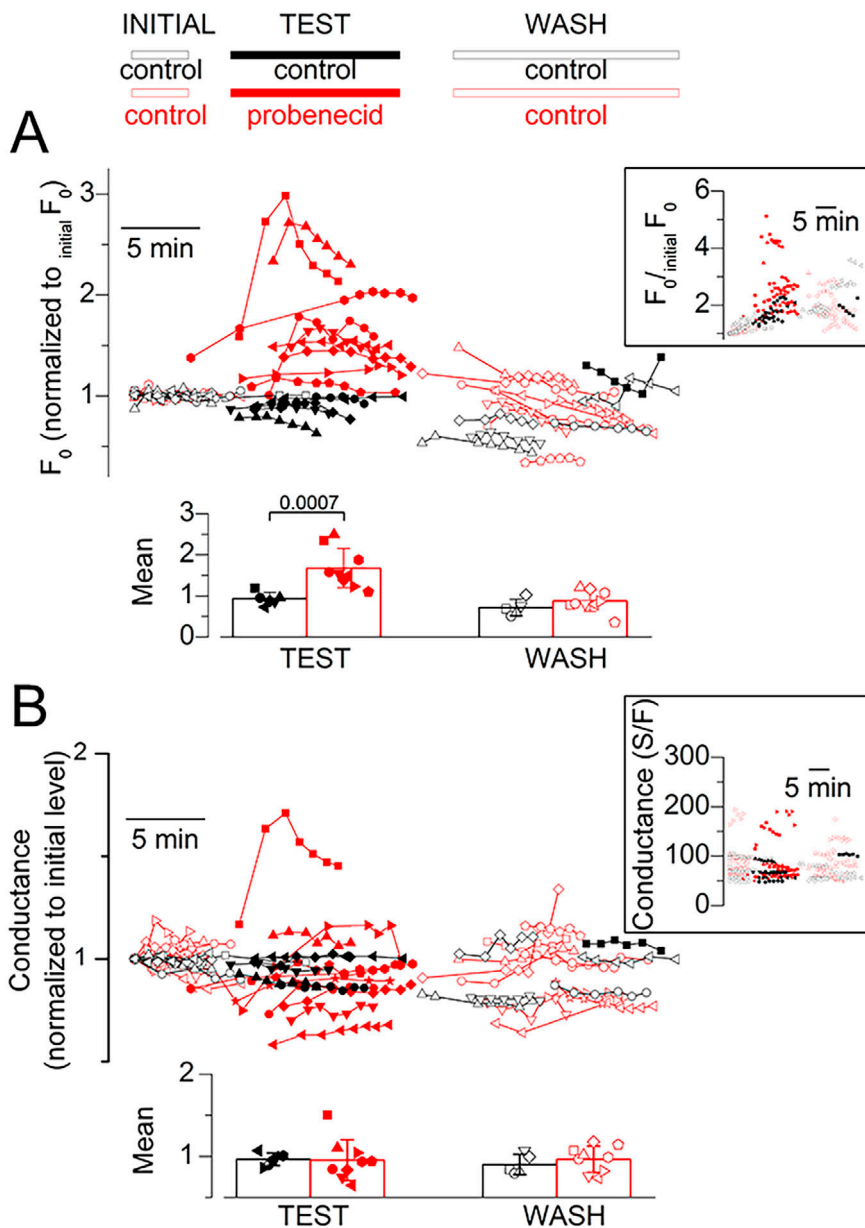
Figure 6. **Effect of probenecid on resting Ca²⁺ and resting membrane conductance.** **(A)** Resting rhod-2 fluorescence level (normalized to the initial value; $_{initial}F_0$) along the course of experiments designed to test the effect of acute application of probenecid. As the exact timing of pulses delivery and of probenecid (or control solution) application and wash-out were not identical for all experiments, data points from each and every fiber tested are shown, with each symbol type corresponding to a distinct fiber. Red symbols are from fibers challenged with probenecid. Black symbols are from fibers challenged with the control protocol. Open symbols correspond to data collected before application and after wash-out of the test solution (probenecid or control), whereas corresponding filled symbols show data collected in the presence of the test solution. The inset shows the raw data while the main panel shows the same data after normalization by a linear function fitted to the data points before the application of probenecid (see the text describing Fig. 6 for details). In one control fiber (squares), depolarizing pulses in the presence of the test-control (DMSO containing) solution were applied much later than in all other fibers and wash-out was not implemented. The bar graphs at the bottom show the mean (±SD) values for $F_0/_{initial}F_0$ calculated from the above datasets, during probenecid (or DMSO for the control experiments) application and after wash. For this, for each fiber, all $F_0/_{initial}F_0$ values obtained (1) during the test period and (2) after wash were averaged. Data are from six fibers from three mice (control) and nine fibers from four mice (probenecid). **(B)** Resting membrane conductance along the course of the same experiments as in A, assessed from the change in membrane current elicited by a 20-mV hyperpolarization from the holding voltage. The inset shows the raw values while the main graph shows the values normalized to the initial conductance level. The bar graphs at the bottom show the mean (±SD) values for normalized conductance calculated from the above datasets during probenecid (or DMSO) application and after wash.

~2 min, following probenecid application (see Fig. 6 A). If this resulted from rhod-2 leakage block, it would mean that, in normal conditions, we would be losing approximately half the cytosolic dye concentration every 2 min, and that this would be balanced by dye diffusion from the voltage-clamp pipette so that concentration is maintained constant or is slightly increasing. This is most unlikely. Furthermore, we have evidence from our previous experience that there is no detectable dye leak in the extracellular space, including a history of experiments performed with dyes pressure-microinjected in isolated fibers, during which dye concentration remained very stable over the course of the experiments (e.g., Collet and Jacquemond, 2002). Overall, the probenecid-induced rise in resting rhod-2 fluorescence is obviously due to a rise in cytosolic Ca²⁺.

We previously reported several experimental situations associated with a use-dependent increase in resting Ca²⁺ triggered upon EC coupling activation. This was due to SR Ca²⁺ leak through RyR1 channels that failed to close, once opened upon membrane depolarization, in the presence of the triggering agent (Collet and Jacquemond, 2002; Pouvreau et al., 2004; Pouvreau et al., 2006). This was not the case here: following the probenecid-induced rise in Ca²⁺, there was no sign of further incremental change in resting Ca²⁺ upon application of depolarizing pulses (Fig. 5 and Fig. 8).

Throughout this series of measurements, each depolarizing pulse was preceded by a 20-mV hyperpolarizing pulse to check for possible changes in resting membrane conductance. Corresponding data are shown in Fig. 6 B: the inset shows the raw values while the main graph shows the same data after
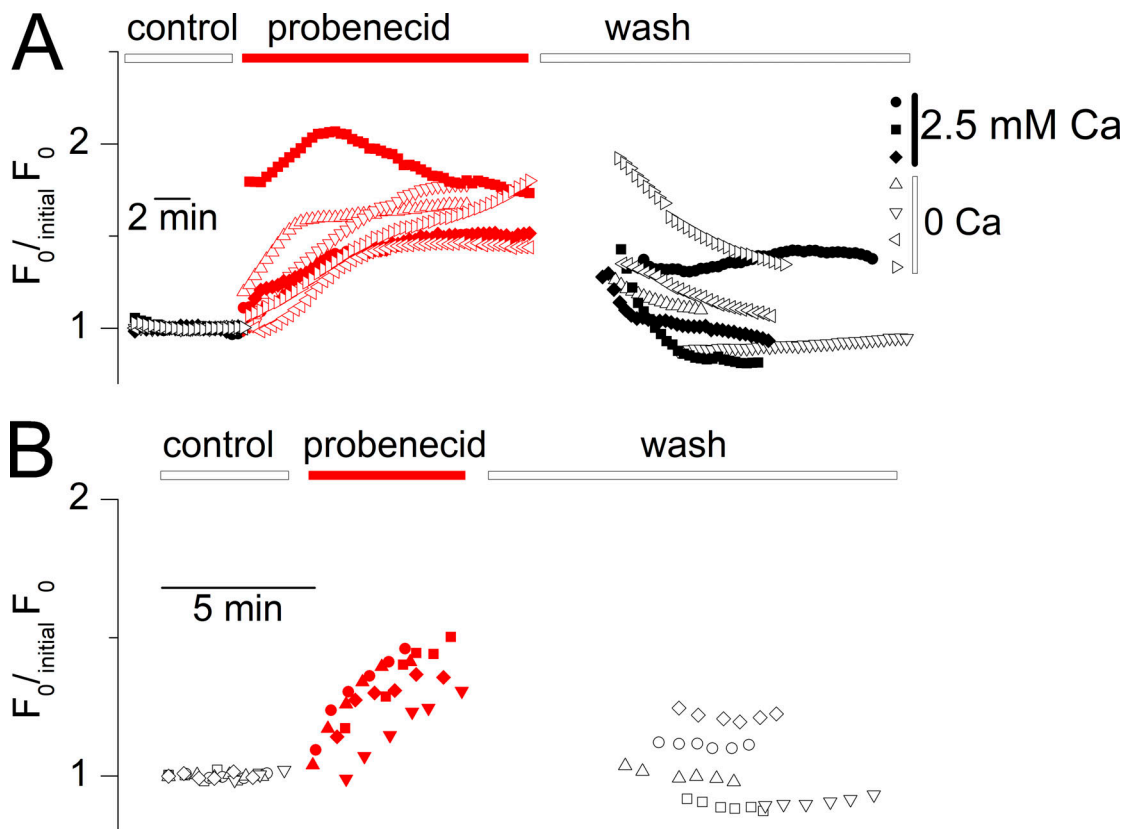
Figure 7. **The probenecid-induced cytosolic Ca²⁺ elevation persists in the absence of extracellular calcium and under voltage-inactivated conditions.** **(A)** Time course of probenecid-induced increase in fluo-4 fluorescence in three fibers bathed in the presence of calcium-containing Tyrode solution (circles) and in four fibers bathed in calcium-deprived Tyrode (triangles). **(B)** Probenecid-induced rise in rhod-2 fluorescence in five muscle fibers voltage-clamped at a holding voltage of −10 mV. Datasets were corrected, as in Fig. 6, by normalization with a linear function fitted to the data points before the application of the drug.

normalization by the initial conductance value at the beginning of the experiment. One probenecid-treated fiber (red squares) did exhibit an increase in membrane conductance during the drug application, which was also accompanied by an inward shift of the holding current of ∼0.2 A/F. However, other fibers did not show a uniform trend of change in membrane conductance, which we took as an indication that the probenecid-induced rise in resting Ca²⁺ was not associated with electrogenic Ca²⁺ entry across the plasma/t-tubule membrane. The bottom graphs in Fig. 6 B report the mean relative change in membrane conductance during probenecid (or control solution) application and after wash-out. Statistical analysis revealed no difference between the control and the probenecid group of fibers in the two conditions.

To further check this point, measurements were carried out in four fibers in the nominal absence of extracellular Ca²⁺. To simplify the conditions, this was performed without a voltage clamp but with muscle fibers bathed in the presence of Tyrode solution and loaded with the Ca²⁺-sensitive dye fluo-4 (see Materials and methods). Probenecid application in that situation still produced an increase in resting fluorescence (Fig. 7 A), although in five other fibers this could not be reliably followed because it was accompanied by an irreversible contracture.

Since RyR1-mediated SR Ca²⁺ release gets inactivated upon prolonged t-tubule membrane depolarization (Hodgkin and Horowicz, 1960), it was also of interest to check whether probenecid would raise resting Ca²⁺ in that situation. For this, rhod-2 fluorescence was measured as in Fig. 6, but in fibers held at a holding voltage of −10 mV, from which depolarizing pulses no more elicit Ca²⁺ release. Fig. 7 B shows corresponding values for $F_0/_{initial}F_0$ along the course of the experiments. Probenecid still elicited a rise in resting Ca²⁺ in the voltage-inactivated fibers.

Probenecid simultaneously affects resting Ca²⁺ homeostasis and SR Ca²⁺ release

Typical changes in SR Ca²⁺ release over the course of the acute probenecid application protocol and of the corresponding control protocol are shown in Fig. 8, B and A, respectively. The two series of traces in Fig. 8, A and B correspond to the rhod-2 fluorescence records (F_0 unit) and the corresponding dCa_{Tot}/dt (µM.ms⁻¹ unit), respectively. The voltage-clamp pulses are shown on the top. The rhod-2 fluorescence records were all normalized to the F_0 level of the first record. The control experiment (Fig. 8 A) shows that there was some run-down in SR Ca²⁺ release over time. Nevertheless, probenecid under the same protocol conditions severely depressed the amplitude of SR Ca²⁺ release, with a limited sign of reversion upon wash out (Fig. 8 B).
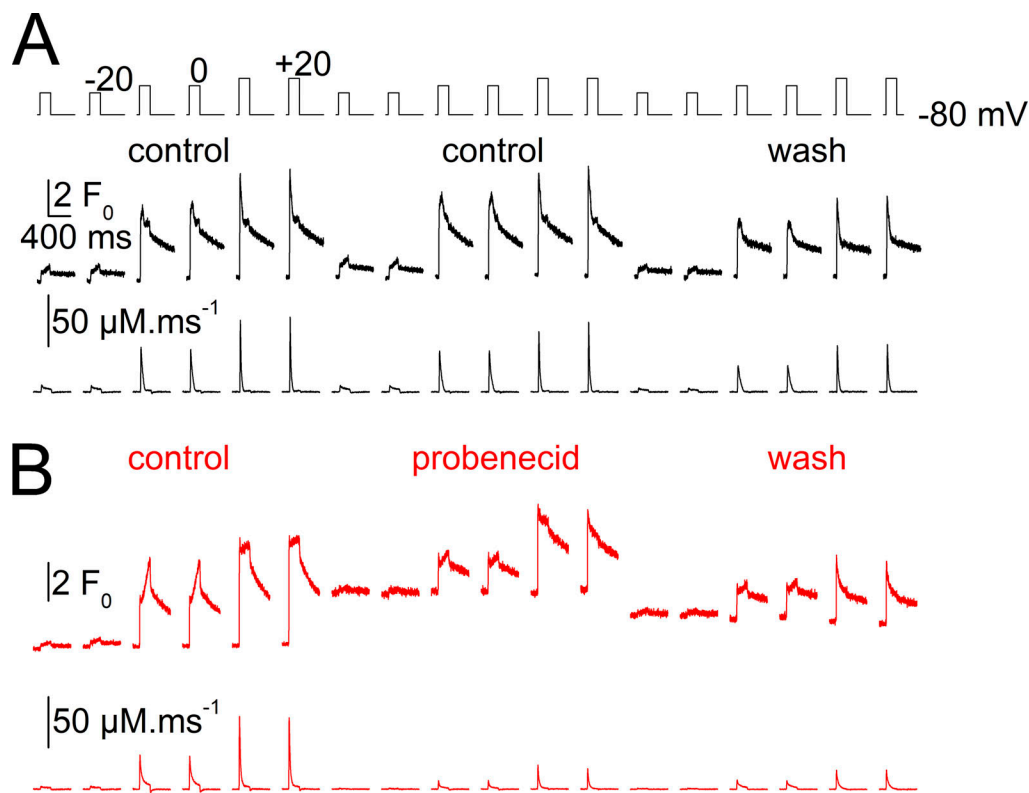
Figure 8.   **Changes in voltage-activated SR Ca²⁺ release flux during probenecid application.** Data are from the same experiments as in Fig. 6. **(A)** Control experiment: rhod-2 Ca²⁺ transients (top, $_{initial}F_0$ unit) and corresponding SR Ca²⁺ release flux (bottom, $\mu M.ms^{-1}$) recorded in response to the voltage pulses shown at the top in a muscle fiber challenged by the test-control protocol (DMSO application) and after wash. **(B)** Test experiment, same measurements as in A from a muscle fiber challenged with probenecid and after wash.

This effect was concomitant with the increase in resting rhod-2 fluorescence, which was partially reversible upon probenecid wash-out. The lack of recovery of SR Ca²⁺ release upon wash-out was likely due to the combination of run-down and only partial reversibility of probenecid effects on the time scale of the experiment.

Fig. 9 shows mean and individual values for the relative changes in peak dCa_{Tot}/dt during the test-control protocol (left) and during probenecid application (right). In each fiber, values for the peak dCa_{Tot}/dt in response to each consecutive pair of pulses of identical amplitude (to −20, 0, and +20 mV) were averaged and normalized to the value measured in response to the first pair of pulses at the same voltage (in the initial control condition). Due to run-down, the relative amplitude of the peak dCa_{Tot}/dt at the end of the experiments (wash) was similarly depressed in both the control and probenecid experiments to ~50% of the initial value. However, for the three tested voltages, the peak dCa_{Tot}/dt amplitude was significantly lower during probenecid application than during the application of the control solution. These results demonstrate that probenecid concomitantly alters resting Ca²⁺ homeostasis and voltage-activated SR Ca²⁺ release.

Probenecid depresses muscle force
The effects of probenecid on SR Ca²⁺ release prompted us to check whether muscle force production is affected by the drug.

For this, resting tension and electrically triggered tetanic contractions were measured in isolated mouse EDL muscles. Results from five EDL muscles tested in the control situation (black symbols) and in probenecid (red symbols) are shown in Fig. 10, B and C. Tension values were normalized by muscle weight. Graphs in Fig. 10, B and C show results from the resting and tetanic tension measurements, respectively, with the right-most graphs reporting the corresponding mean values. As compared with the control measurements, the application of probenecid generated a substantial drop in peak tetanic tension at times 30 and 45 min following drug application, while resting tension was enhanced at 45 min.

Discussion
We demonstrate that probenecid affects muscle function through perturbation of Ca²⁺ homeostasis and EC coupling. Beyond the specific interest in terms of underlying cellular mechanisms and physiological outcomes, these results are also relevant to the use of probenecid in clinics as they raise the possibility that some treated patients may experience altered muscle function. Furthermore, results are also relevant in terms of general functional impact for cellular homeostasis since probenecid-induced changes in Ca²⁺ regulation may be shared by other tissues that are therapeutic targets of this drug.
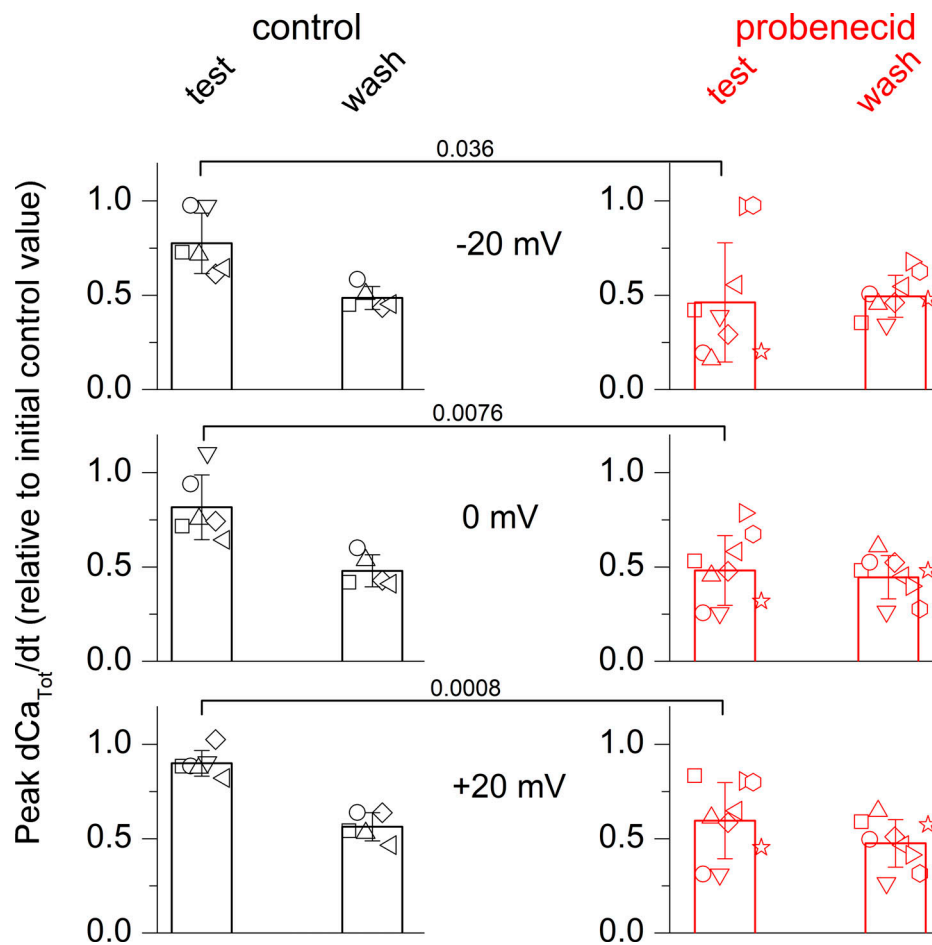
Figure 9. **Relative change in the amplitude of peak SR Ca²⁺ release flux following probenecid (or control solution) application and wash-out.** Data are from the same experiments as in Fig. 6. Individual values from each fiber, and corresponding mean (±SD) values, for the relative change in peak SR Ca²⁺ release flux following application of the control solution (control-test, left) or of the probenecid-containing solution (probenecid-test, right) and after wash-out. Values in each fiber were normalized to the corresponding peak SR Ca²⁺ release flux in the initial control condition. Graphs from top to bottom report the changes at the three tested voltages.

One limitation of our study is that we only used muscles and muscle fibers isolated from male mice. At present, we cannot exclude that findings would differ if using samples from female mice, and this is all the more important in the light of previously reported gender-related differences in the consequences of Panx1 deficiency and/or Panx1 pharmacological blockade on other physiological responses (Freitas-Andrade et al., 2017; Aguilar-Perez et al., 2019).

Probenecid has had a history of clinical use for its potency to inhibit organic anion transporters, making it efficient as a uricosuric agent for gout treatment (Gutman and Yu, 1951; Roch-Ramel et al., 1997) and as an adjuvant to increase the concentration of antibiotics and chemotherapeutic agents (e.g., Burnell and Kirby, 1951). There are also repositioning perspectives for its use as an antiviral and anticancer agent (Ahmed et al., 2016) and also because of its potency to block inflammasome activation (Dahl and Keane, 2012). In this context, the potential benefit of probenecid as a therapeutic agent has been considered for trauma and stroke in the central nervous system and also for disease situations such as multiple sclerosis (Hainz et al., 2017) and SARS-CoV-2 infection (Murray et al., 2021).

Probenecid also gained popularity within the sport performance doping field, presumably because of its capacity to reduce the excretion of anabolic-androgenic steroids (Hemmersbach, 2020). Nonetheless, to mention that the exact conditions of dosing for that particular purpose remain poorly documented. In healthy volunteers, a single 2.0-g oral dose (which is a commonly prescribed daily dosage for adult patients) was shown to result in a peak plasma level in the half-millimolar range, and higher levels may be reached under conditions of repeated dosing (Selen et al., 1982).

Under our conditions, concentration levels of probenecid in the millimolar range reduce the amplitude of voltage-activated SR Ca²⁺ release, which has to make a major contribution to the probenecid-induced reduction of whole-muscle contraction. Fiber-to-fiber variability limited our capability to identify a probenecid effect at a lower dose. Variability may be related, at least in part, to the presence of several fiber types in the FDB muscle (see for instance Calderon et al., 2009; Banas et al., 2011), and we also cannot exclude that fibers of distinct types present with a different susceptibility to probenecid.
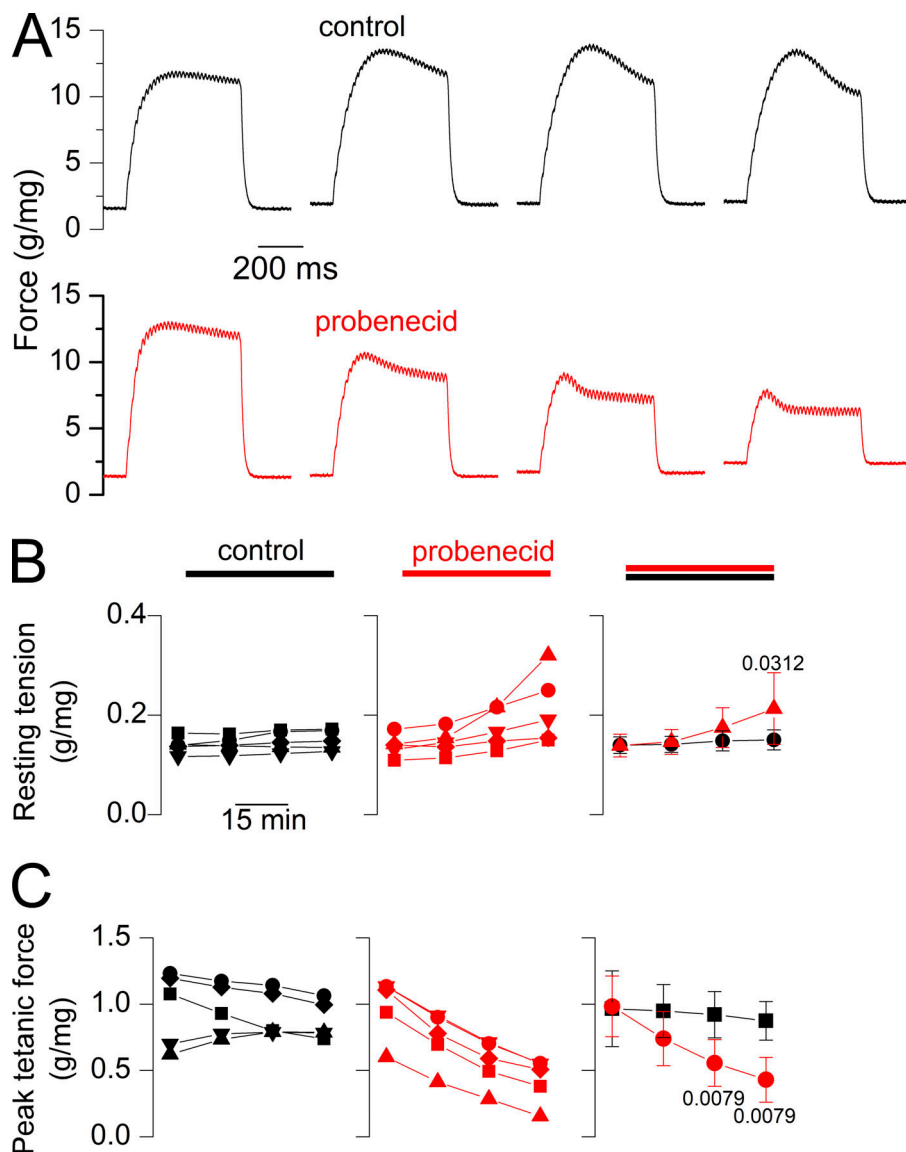
Figure 10. Effect of probenecid on whole muscle resting and tetanic tension. (A) Representative records of the tension response of an isolated EDL muscle to a 60-Hz train of field stimulation applied every 15 min. Following the first train, the extracellular Ringer solution was replaced by the same solution containing either only DMSO (top) or probenecid (bottom). **(B)** Resting tension from five isolated EDL muscles electrically stimulated as in Fig. 10 A, and challenged either with the control protocol (black) or with probenecid (red). In both groups, the first measurement was taken in the presence of the control Ringer solution. The right-most graph shows the mean (±SD) values from the two groups. **(C)** Corresponding results for the peak amplitude of the tetanic tension. Note that in these whole muscle experiments, the course of probenecid equilibration within the entire section of the muscle is likely to take much longer than in the single muscle fibers experiments. In addition, contraction of the muscle may favor intramuscle equilibration of the drug and promote its effect, making it look like a use-dependent effect.

Probenecid also induces Ca^{2+} release from an intracellular store at rest, which may be responsible for the increase in muscle resting tension. In our experiments with rhod-2, we estimated that probenecid elevated the resting cytosolic free Ca^{2+} level by ∼0.1–0.2 μM. Considering that this elevation was achieved in the presence of millimolar levels of intracellular EGTA, the total amount of released Ca^{2+} was much more than the change in free Ca^{2+}, likely within the several hundreds of micromolar to millimolar range. This has two major implications: first, the corresponding intracellular store has to be the SR, as there is no other compartment in muscle with such Ca^{2+} storage capacity. Second, the SR had to become, to some extent, Ca^{2+}-depleted, upon probenecid application, and this is expected to contribute to, if not to fully underlie, the associated depression of voltage-activated SR Ca^{2+} release. To address whether SR Ca^{2+} content is reduced in probenecid-treated fibers, we compared the time course of Ca^{2+} release between control fibers and probenecid-treated fibers exhibiting a similar initial peak value of Ca^{2+} release. A comparison was made between the batch of muscle fibers treated with 2 mM

probenecid and the corresponding batch of control fibers (Fig. 2). Fig. 11 shows individual traces of Ca^{2+} release flux (A) and corresponding total released Ca^{2+} (B) from control fibers and probenecid-treated fibers, selected for exhibiting a similar level of initial peak SR Ca^{2+} release. Results clearly show that the slowly decaying phase in the control fibers was absent in the probenecid-treated fibers, consistent with rapid SR Ca^{2+} depletion during the voltage pulse in the presence of probenecid.

It is noteworthy that Panx1 knockdown was also associated with depressed SR Ca^{2+} release but with maintained SR Ca^{2+} content (Jaque-Fernandez et al., 2021). We believe this is not inconsistent as no straightforward mechanistic parallel can be made between acute treatment with probenecid and Panx1 removal. Also, Panx1 knockdown was achieved through plasmid-electroporation in vivo, followed by a period of 2 wk before measurements were taken. Over the course of that period, there was certainly a possibility for changes in resting Ca^{2+} but also for adaptative changes in Ca^{2+} homeostasis that would not occur under acute drug treatment.
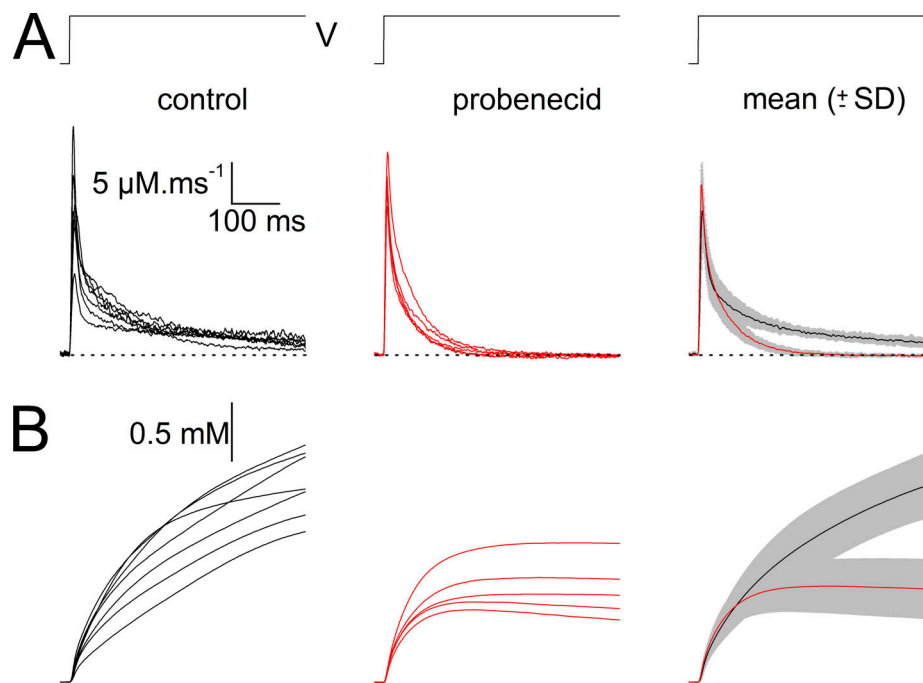
Figure 11. Evidence for reduced SR Ca²⁺ content in probenecid-treated fibers. (A) Individual traces of Ca²⁺ release flux from control fibers (left, seven fibers from three mice) and from fibers treated with 2 mM probenecid (middle, five fibers from two mice). The right panel shows the corresponding mean (±SD, grey shading) time course of Ca²⁺ release. Data are from the same group of fibers as in Fig. 2. Traces in the two groups were selected on the basis of their similar value for initial peak Ca²⁺ release flux of ~20 µM.ms⁻¹, irrespective of the activation voltage. Notice that, following the initial peak, the Ca²⁺ release flux decreases to zero in the probenecid-treated fibers whereas a slowly decaying phase persists in the control fibers. **(B)** Time course of the total released Ca²⁺ calculated from the above traces in A. Total released Ca²⁺ rapidly reaches a steady level in the probenecid-treated fibers, whereas it keeps rising in the control fibers.

Three major mechanisms of action for probenecid have so far been reported. Probenecid inhibits organic anion transporters, but we hardly see how this could be involved in alterations of Ca²⁺ homeostasis and EC coupling. Probenecid is an agonist of TRPV2 channels (Bang et al., 2007). In cardiac cells, TRPV2 operates as a mechanosensitive channel involved in Ca²⁺ entry across the sarcolemma (see Entin-Meer and Keren, 2020) with a potentially important role in normal heart function (Rubinstein et al., 2014). Of interest in this context, probenecid-induced TRPV2 activation was shown to improve cardiac function in patients with heart failure (Robbins et al., 2018). In skeletal muscle, TRPV2 in the plasma membrane also operates as a mechanosensitive channel, involved in osmo-sensation, capable of contributing to t-tubule membrane depolarization and consequent SR Ca²⁺ release (Zanou et al., 2015). However, in this configuration, TRPV2 is certainly not involved in the effects we report here on Ca²⁺ homeostasis because (1) the voltage-clamp conditions preclude any TRPV2 activation-induced membrane depolarization and consequent SR Ca²⁺ release, (2) we found no reproducible evidence for a probenecid-induced increase in membrane conductance, (3) the probenecid-induced rise in cytosolic Ca²⁺ persisted in the absence of extracellular calcium.

The third major target of probenecid is the membrane channel protein Panx1 (Silverman et al., 2008), involved in ATP release out to the extracellular space and consequent activation of purinergic receptors. Under our conditions, probenecid-induced block of Panx1-mediated ATP release could then be speculated to play a role in the altered Ca²⁺ homeostasis. This is however unlikely because the effect was not shared by the ¹⁰panx1 blocker and also because this would mean that a chronic feedback of released ATP-induced purinergic signaling operates on RyR1-mediated SR Ca²⁺ release, which would be essential for proper EC coupling function. This is hardly workable, as also confirmed by the absence of the effect of a P2Y2 antagonist on SR Ca²⁺ release.

An alternative relies on the fact that Panx1 is part of a protein complex including Ca$_V$1.1 (Arias-Calderón et al., 2016). One could then consider the possibility that probenecid binding to Panx1 modifies protein–protein interactions within this complex, so as to alter proper control of RyR1 function. This would concur with the proposal that Panx1 removal disrupts the proper organization and/or function of the Ca$_V$1.1–RyR1 interactions (Jaque-Fernandez et al., 2021). Probenecid is believed to bind to extracellular loop 1 of Panx1, and probenecid-bound Panx1 was suggested to experience changes in conformation, including bending of the N-terminal region toward the cytoplasm and modification of the tilt angle of each subunit relative to the membrane plane, in addition to occlusion of the pore (Kuzuya et al., 2022). Accordingly, one could speculate that these changes in Panx1 conformation alter proper interactions within the denoted protein complex. Nevertheless, there was no indication that Ca$_V$1.1 charge movement is altered by probenecid. Furthermore, probenecid was still capable of inducing SR Ca²⁺ release in fibers maintained at a depolarized voltage that

inactivates $Ca_V1.1$ (Fig. 7 B). Thus, the mechanism of probenecid-induced Ca^{2+} leak bypasses the control of RyR1 by $Ca_V1.1$. We thus cannot exclude that probenecid acts by a mechanism totally independent from its capacity to bind Panx1, as for instance a direct effect on the RyR1 channel protein. In that regard, there was no use-dependence of the probenecid-induced SR Ca^{2+} leak, which means that RyR1 channel opening does not promote the efficiency of the drug.

Carbenoxolone also blocks the Panx1 channel pore by binding to a motif of the extracellular domain (Ruan et al., 2020; Jin et al., 2020; Mim et al., 2021), but no associated detectable change in Panx1 conformation was detected (Jin et al., 2020), thus limiting the view that carbenoxolone acts on SR Ca^{2+} release because of a change in Panx1 conformation. Still, distinctly from probenecid, our estimates of charge movement were depressed in the presence of carbenoxolone so that a direct or indirect effect on $Ca_V1.1$ may be involved in its potency to affect SR Ca^{2+} release.

Irrespective of the mechanism, our results provide strong evidence that probenecid alters muscle Ca^{2+} homeostasis so as to affect muscle force production. There is no straightforward report in the literature of muscle weakness and/or muscle fatiguability as consequences of probenecid treatment, although "unusual tiredness or weakness" are stated as potential side effects of the drug by the commercial providers. It may then well be that consequences for muscle function in patients are either none or negligible. This could be due to a variety of reasons, a major one being that the effect requires levels greater than the commonly expected blood concentration in clinical use (0.07–0.7 mM range; Schulz et al., 2020). Alternatively, it may also be that any moderate effect on muscle has remained undetected because the disease status of the treated patients does not favor clear-cut identification of altered muscle function. In contrast, however, an adverse side effect of probenecid on muscle function should have had more chances to be identified in the context of doping in sport. In any case, our results should tend to discourage probenecid use when looking for improved muscle performance.

Acknowledgments

References

Aguilar-Perez, A., R. Pacheco-Costa, E.G. Atkinson, P. Deosthale, H.M. Davis, A.L. Essex, J.E. Dilley, L. Gomez, J.E. Rupert, T.A. Zimmers, et al. 2019. Age- and sex-dependent role of osteocytic pannexin1 on bone and muscle mass and strength. *Sci. Rep.* 9:13903. https://doi.org/10.1038/s41598-019-50444-1

Ahmed, M.U., D.J. Bennett, T.C. Hsieh, B.B. Doonan, S. Ahmed, and J.M. Wu. 2016. Repositioning of drugs using open-access data portal DTome: A test case with probenecid (review). *Int. J. Mol. Med.* 37:3–10. https://doi.org/10.3892/ijmm.2015.2411

Arias-Calderón, M., G. Almarza, A. Díaz-Vegas, A. Contreras-Ferrat, D. Valladares, M. Casas, H. Toledo, E. Jaimovich, and S. Buvinic. 2016. Characterization of a multiprotein complex involved in excitation-transcription coupling of skeletal muscle. *Skelet. Muscle.* 6:15. https://doi.org/10.1186/s13395-016-0087-5

Banas, K., C. Clow, B.J. Jasmin, and J.M. Renaud. 2011. The KATP channel Kir6.2 subunit content is higher in glycolytic than oxidative skeletal muscle fibers. *Am. J. Physiol. Regul. Integr. Comp. Physiol.* 301:R916–R925. https://doi.org/10.1152/ajpregu.00663.2010

Bang, S., K.Y. Kim, S. Yoo, S.H. Lee, and S.W. Hwang. 2007. Transient receptor potential V2 expressed in sensory neurons is activated by probenecid. *Neurosci. Lett.* 425:120–125. https://doi.org/10.1016/j.neulet.2007.08.035

Burnell, J.M., and W.M. Kirby. 1951. Effectiveness of a new compound, benemid, in elevating serum penicillin concentrations. *J. Clin. Invest.* 30:697–700. https://doi.org/10.1172/JCI102482

Bustamante, M., R. Fernández-Verdejo, E. Jaimovich, and S. Buvinic. 2014. Electrical stimulation induces IL-6 in skeletal muscle through extracellular ATP by activating Ca^{2+} signals and an IL-6 autocrine loop. *Am. J. Physiol. Endocrinol. Metab.* 306:E869–E882. https://doi.org/10.1152/ajpendo.00450.2013

Buvinic, S., G. Almarza, M. Bustamante, M. Casas, J. López, M. Riquelme, J.C. Sáez, J.P. Huidobro-Toro, and E. Jaimovich. 2009. ATP released by electrical stimuli elicits calcium transients and gene expression in skeletal muscle. *J. Biol. Chem.* 284:34490–34505. https://doi.org/10.1074/jbc.M109.057315

Calderón, J.C., P. Bolaños, S.H. Torres, G. Rodríguez-Arroyo, and C. Caputo. 2009. Different fibre populations distinguished by their calcium transient characteristics in enzymatically dissociated murine flexor digitorum brevis and soleus muscles. *J. Muscle Res. Cell Motil.* 30:125–137. https://doi.org/10.1007/s10974-009-9181-1

Casas, M., R. Figueroa, G. Jorquera, M. Escobar, J. Molgó, and E. Jaimovich. 2010. IP_3-dependent, post-tetanic calcium transients induced by

Jaque-Fernandez et al.
Probenecid impairs excitation–contraction coupling

Journal of General Physiology
https://doi.org/10.1085/jgp.202213203

15 of 17

electrostimulation of adult skeletal muscle fibers. *J. Gen. Physiol.* 136: 455–467. https://doi.org/10.1085/jgp.200910397

Collet, C., and V. Jacquemond. 2002. Sustained release of calcium elicited by membrane depolarization in ryanodine-injected mouse skeletal muscle fibers. *Biophys. J.* 82:1509–1523. https://doi.org/10.1016/S0006-3495(02)75504-5

Collet, C., S. Pouvreau, L. Csernoch, B. Allard, and V. Jacquemond. 2004. Calcium signaling in isolated skeletal muscle fibers investigated under "silicone voltage-clamp" conditions. *Cell Biochem. Biophys.* 40:225–236. https://doi.org/10.1385/CBB:40:2:225

Curtis, M.J., S. Alexander, G. Cirino, J.R. Docherty, C.H. George, M.A. Giembycz, D. Hoyer, P.A. Insel, A.A. Izzo, Y. Ji, et al. 2018. Experimental design and analysis and their reporting II: Updated and simplified guidance for authors and peer reviewers. *Br. J. Pharmacol.* 175:987–993. https://doi.org/10.1111/bph.14153

Dahl, G., F. Qiu, and J. Wang. 2013. The bizarre pharmacology of the ATP release channel pannexin1. *Neuropharmacology.* 75:583–593. https://doi.org/10.1016/j.neuropharm.2013.02.019

Dahl, G. 2015. ATP release through pannexon channels. *Philos. Trans. R. Soc. Lond. B Biol. Sci.* 370:20140191. https://doi.org/10.1098/rstb.2014.0191

Dahl, G. 2018. The Pannexin1 membrane channel: Distinct conformations and functions. *FEBS Lett.* 592:3201–3209. https://doi.org/10.1002/1873-3468.13115

Dahl, G., and R.W. Keane. 2012. Pannexin: From discovery to bedside in 11±4 years? *Brain Res.* 1487:150–159. https://doi.org/10.1016/j.brainres.2012.04.058

Di Virgilio, F., C. Fasolato, and T.H. Steinberg. 1988. Inhibitors of membrane transport system for organic anions block fura-2 excretion from PC12 and N2A cells. *Biochem. J.* 256:959–963. https://doi.org/10.1042/bj2560959

Eisner, D.A. 2021. Pseudoreplication in physiology: More means less. *J. Gen. Physiol.* 153:e202012826. https://doi.org/10.1085/jgp.202012826

Entin-Meer, M., and G. Keren. 2020. Potential roles in cardiac physiology and pathology of the cation channel TRPV2 expressed in cardiac cells and cardiac macrophages: A mini-review. *Am. J. Physiol. Heart Circ. Physiol.* 318:H181–H188. https://doi.org/10.1152/ajpheart.00491.2019

Eugenin, E.A. 2014. Role of connexin/pannexin containing channels in infectious diseases. *FEBS Lett.* 588:1389–1395. https://doi.org/10.1016/j.febslet.2014.01.030

Freitas-Andrade, M., J.F. Bechberger, B.A. MacVicar, V. Viau, and C.C. Naus. 2017. Pannexin1 knockout and blockade reduces ischemic stroke injury in female, but not in male mice. *Oncotarget.* 8:36973–36983. https://doi.org/10.18632/oncotarget.16937

García, J., K. McKinley, S.H. Appel, and E. Stefani. 1992. Ca²⁺ current and charge movement in adult single human skeletal muscle fibres. *J. Physiol.* 454:183–196. https://doi.org/10.1113/jphysiol.1992.sp019259

Giaume, C., C.C. Naus, J.C. Sáez, and L. Leybaert. 2021. Glial connexins and pannexins in the healthy and diseased brain. *Physiol. Rev.* 101:93–145. https://doi.org/10.1152/physrev.00043.2018

Gutman, A.B., and T.F. Yu. 1951. Benemid (p-di-n-propylsulfamyl)-benzoic acid) as uricosuric agent in chronic gouty arthritis. *Trans. Assoc. Am. Physicians.* 64:279–288.

Hainz, N., S. Wolf, A. Beck, S. Wagenpfeil, T. Tschernig, and C. Meier. 2017. Probenecid arrests the progression of pronounced clinical symptoms in a mouse model of multiple sclerosis. *Sci. Rep.* 7:17214. https://doi.org/10.1038/s41598-017-17517-5

Hemmersbach, P. 2020. The Probenecid-story: A success in the fight against doping through out-of-competition testing. *Drug Test. Anal.* 12:589–594. https://doi.org/10.1002/dta.2727

Hernández-Ochoa, E.O., and M.F. Schneider. 2012. Voltage clamp methods for the study of membrane currents and SR Ca²⁺ release in adult skeletal muscle fibres. *Prog. Biophys. Mol. Biol.* 108:98–118. https://doi.org/10.1016/j.pbiomolbio.2012.01.001

Hernández-Ochoa, E.O., and M.F. Schneider. 2018. Voltage sensing mechanism in skeletal muscle excitation-contraction coupling: Coming of age or midlife crisis? *Skelet. Muscle* 8:22. https://doi.org/10.1186/s13395-018-0167-9

Hodgkin, A.L., and P. Horowicz. 1960. Potassium contractures in single muscle fibres. *J. Physiol.* 153:386–403. https://doi.org/10.1113/jphysiol.1960.sp006541

Ito, N., U.T. Ruegg, and S. Takeda. 2018. ATP-induced increase in intracellular calcium levels and subsequent activation of mTOR as regulators of skeletal muscle hypertrophy. *Int. J. Mol. Sci.* 19:2804. https://doi.org/10.3390/ijms19092804

Jacquemond, V. 1997. Indo-1 fluorescence signals elicited by membrane depolarization in enzymatically isolated mouse skeletal muscle fibers. *Biophys. J.* 73:920–928. https://doi.org/10.1016/S0006-3495(97)78124-4

Jaque-Fernández, F., B. Allard, L. Monteiro, A. Lafoux, C. Huchet, E. Jaimovich, C. Berthier, and V. Jacquemond. 2022. Probenecid affects sarcoplasmic reticulum Ca²⁺ release and depresses contractile activation in mouse skeletal muscle. *J. Gen. Physiol.* 154:e2021ecc23. https://doi.org/10.1085/jgp.2021ecc23

Jaque-Fernández, F., G. Jorquera, J. Troc-Gajardo, F. Pietri-Rouxel, C. Gentil, S. Buvinic, B. Allard, E. Jaimovich, V. Jacquemond, and M. Casas. 2021. Pannexin-1 and Caᵥ1.1 show reciprocal interaction during excitation-contraction and excitation-transcription coupling in skeletal muscle. *J. Gen. Physiol.* 153:e202012635. https://doi.org/10.1085/jgp.202012635

Jin, Q., B. Zhang, X. Zheng, N. Li, L. Xu, Y. Xie, F. Song, E.A. Bhat, Y. Chen, N. Gao, et al. 2020. Cryo-EM structures of human pannexin 1 channel. *Cell Res.* 30:449–451. https://doi.org/10.1038/s41422-020-0310-0

Jorquera, G., F. Altamirano, A. Contreras-Ferrat, G. Almarza, S. Buvinic, V. Jacquemond, E. Jaimovich, and M. Casas. 2013. Cav1.1 controls frequency-dependent events regulating adult skeletal muscle plasticity. *J. Cell Sci.* 126:1189–1198. https://doi.org/10.1242/jcs.116855

Kutchukian, C., M. Lo Scrudato, Y. Tourneur, K. Poulard, A. Vignaud, C. Berthier, B. Allard, M.W. Lawlor, A. Buj-Bello, and V. Jacquemond. 2016. Phosphatidylinositol 3-kinase inhibition restores Ca²⁺ release defects and prolongs survival in myotubularin-deficient mice. *Proc. Natl. Acad. Sci. USA.* 113:14432–14437. https://doi.org/10.1073/pnas.1604099113

Kuzuya, M., H. Hirano, K. Hayashida, M. Watanabe, K. Kobayashi, T. Terada, M.I. Mahmood, F. Tama, K. Tani, Y. Fujiyoshi, and A. Oshima. 2022. Structures of human pannexin-1 in nanodiscs reveal gating mediated by dynamic movement of the N terminus and phospholipids. *Sci. Signal.* 15: eabg6941. https://doi.org/10.1126/scisignal.abg6941

Lefebvre, R., C. Legrand, E. González-Rodríguez, L. Groom, R.T. Dirksen, and V. Jacquemond. 2011. Defects in Ca²⁺ release associated with local expression of pathological ryanodine receptors in mouse muscle fibres. *J. Physiol.* 589:5361–5382. https://doi.org/10.1113/jphysiol.2011.216408

Li, J., Z. Gao, V. Kehoe, J. Xing, N. King, and L. Sinoway. 2008. Interstitial adenosine triphosphate modulates muscle afferent nerve-mediated pressor reflex. *Muscle Nerve.* 38:972–977. https://doi.org/10.1002/mus.21014

Mackrill, J.J. 2010. Ryanodine receptor calcium channels and their partners as drug targets. *Biochem. Pharmacol.* 79:1535–1543. https://doi.org/10.1016/j.bcp.2010.01.014

Mim, C., G. Perkins, and G. Dahl. 2021. Structure versus function: Are new conformations of pannexin 1 to be resolved? *J. Gen. Physiol.* 153: e202012754. https://doi.org/10.1085/jgp.202012754

Murray, J., R.J. Hogan, D.E. Martin, K. Blahunka, F.D. Sancilio, R. Balyan, M. Lovern, R. Still, and R.A. Tripp. 2021. Probenecid inhibits SARS-CoV-2 replication in vivo and in vitro. *Sci. Rep.* 11:18085. https://doi.org/10.1038/s41598-021-97658-w

Navis, K.E., C.Y. Fan, T. Trang, R.J. Thompson, and D.J. Derksen. 2020. Pannexin 1 channels as a therapeutic target: Structure, inhibition, and outlook. *ACS Chem. Neurosci.* 11:2163–2172. https://doi.org/10.1021/acschemneuro.0c00333

Nyberg, M., B.K. Al-Khazraji, S.P. Mortensen, D.N. Jackson, C.G. Ellis, and Y. Hellsten. 2013. Effect of extraluminal ATP application on vascular tone and blood flow in skeletal muscle: Implications for exercise hyperemia. *Am. J. Physiol. Regul. Integr. Comp. Physiol.* 305:R281–R290. https://doi.org/10.1152/ajpregu.00189.2013

Pelegrin, P., and A. Surprenant. 2006. Pannexin-1 mediates large pore formation and interleukin-1β release by the ATP-gated P2X7 receptor. *EMBO J.* 25:5071–5082. https://doi.org/10.1038/sj.emboj.7601378

Percie du Sert, N., V. Hurst, A. Ahluwalia, S. Alam, M.T. Avey, M. Baker, W.J. Browne, A. Clark, I.C. Cuthill, U. Dirnagl, et al. 2020. The ARRIVE guidelines 2.0: Updated guidelines for reporting animal research. *PLoS Biol.* 18:e3000410. https://doi.org/10.1371/journal.pbio.3000410

Pouvreau, S., B. Allard, C. Berthier, and V. Jacquemond. 2004. Control of intracellular calcium in the presence of nitric oxide donors in isolated skeletal muscle fibres from mouse. *J. Physiol.* 560:779–794. https://doi.org/10.1113/jphysiol.2004.072397

Pouvreau, S., L. Csernoch, B. Allard, J.M. Sabatier, M. De Waard, M. Ronjat, and V. Jacquemond. 2006. Transient loss of voltage control of Ca²⁺ release in the presence of maurocalcine in skeletal muscle. *Biophys. J.* 91: 2206–2215. https://doi.org/10.1529/biophysj.105.078089

Rebbeck, R.T., Y. Karunasekara, P.G. Board, N.A. Beard, M.G. Casarotto, and A.F. Dulhunty. 2014. Skeletal muscle excitation-contraction coupling:

Who are the dancing partners? *Int. J. Biochem. Cell Biol.* 48:28–38. https://doi.org/10.1016/j.biocel.2013.12.001

Ríos, E. 2018. Calcium-induced release of calcium in muscle: 50 years of work and the emerging consensus. *J. Gen. Physiol.* 150:521–537. https://doi.org/10.1085/jgp.201711959

Robbins, N., M. Gilbert, M. Kumar, J.W. McNamara, P. Daly, S.E. Koch, G. Conway, M. Effat, J.G. Woo, S. Sadayappan, and J. Rubinstein. 2018. Probenecid improves cardiac function in patients with heart failure with reduced ejection fraction in vivo and Cardiomyocyte calcium sensitivity in vitro. *J. Am. Heart Assoc.* 7:e007148. https://doi.org/10.1161/JAHA.117.007148

Roch-Ramel, F., B. Guisan, and J. Diezi. 1997. Effects of uricosuric and anti-uricosuric agents on urate transport in human brush-border membrane vesicles. *J. Pharmacol. Exp. Ther.* 280:839–845.

Ruan, Z., I.J. Orozco, J. Du, and W. Lü. 2020. Structures of human pannexin 1 reveal ion pathways and mechanism of gating. *Nature.* 584:646–651. https://doi.org/10.1038/s41586-020-2357-y

Rubinstein, J., V.M. Lasko, S.E. Koch, V.P. Singh, V. Carreira, N. Robbins, A.R. Patel, M. Jiang, P. Bidwell, E.G. Kranias, et al. 2014. Novel role of transient receptor potential vanilloid 2 in the regulation of cardiac performance. *Am. J. Physiol. Heart Circ. Physiol.* 306:H574–H584. https://doi.org/10.1152/ajpheart.00854.2013

Sanchez, C., C. Berthier, Y. Tourneur, L. Monteiro, B. Allard, L. Csernoch, and V. Jacquemond. 2021. Detection of Ca^{2+} transients near ryanodine receptors by targeting fluorescent Ca^{2+} sensors to the triad. *J. Gen. Physiol.* 153:e202012592. https://doi.org/10.1085/jgp.202012592

Schulz, M., A. Schmoldt, H. Andresen-Streichert, and S. Iwersen-Bergmann. 2020. Revisited: Therapeutic and toxic blood concentrations of more than 1100 drugs and other xenobiotics. *Crit. Care.* 24:195. https://doi.org/10.1186/s13054-020-02915-5

Selen, A., G.L. Amidon, and P.G. Welling. 1982. Pharmacokinetics of probenecid following oral doses to human volunteers. *J. Pharm. Sci.* 71:1238–1242. https://doi.org/10.1002/jps.2600711114

Silverman, W., S. Locovei, and G. Dahl. 2008. Probenecid, a gout remedy, inhibits pannexin 1 channels. *Am. J. Physiol. Cell Physiol.* 295:C761–C767. https://doi.org/10.1152/ajpcell.00227.2008

Struk, A., F. Lehmann-Horn, and W. Melzer. 1998. Voltage-dependent calcium release in human malignant hyperthermia muscle fibers. *Biophys. J.* 75:2402–2410. https://doi.org/10.1016/S0006-3495(98)77684-2

Vultaggio-Poma, V., A.C. Sarti, and F. Di Virgilio. 2020. Extracellular ATP: A feasible target for cancer therapy. *Cells.* 9:2496. https://doi.org/10.3390/cells9112496

Wang, N., M. De Bock, E. Decrock, M. Bol, A. Gadicherla, M. Vinken, V. Rogiers, F.F. Bukauskas, G. Bultynck, and L. Leybaert. 2013. Paracrine signaling through plasma membrane hemichannels. *Biochim. Biophys. Acta.* 1828:35–50. https://doi.org/10.1016/j.bbamem.2012.07.002

Whyte-Fagundes, P., and G. Zoidl. 2018. Mechanisms of pannexin1 channel gating and regulation. *Biochim. Biophys. Acta Biomembr.* 1860:65–71. https://doi.org/10.1016/j.bbamem.2017.07.009

Zanou, N., L. Mondin, C. Fuster, F. Seghers, I. Dufour, M. de Clippele, O. Schakman, N. Tajeddine, Y. Iwata, S. Wakabayashi, et al. 2015. Osmosensation in TRPV2 dominant negative expressing skeletal muscle fibres. *J. Physiol.* 593:3849–3863. https://doi.org/10.1113/JP270522